Available online at www.sciencedirect.com
ScienceDirect
Journal of Power Sources 164 (2007) 141–153
JOURNAL OF POWER SOURCES
www.elsevier.com/locate/jpowsour

Gas diffusion layer durability under steady-state and freezing conditions

Charles Lee, Walter Mérida *

Clean Energy Research Centre (CERC), University of British Columbia, 6250 Applied Science Lane, Vancouver, BC, Canada V6T 1Z4

Received 26 July 2006; received in revised form 28 August 2006; accepted 15 September 2006
Available online 17 November 2006

Abstract

In this study, GDL compressive strain under steady-state and freezing conditions, and the effects of freezing conditions on GDL properties of electrical resistivity, bending stiffness, air permeability, surface contact angle, porosity and water vapor diffusion were studied. GDL strain was measured to occur under steady-state aging conditions (80 °C and 200 psi). A maximum strain of 0.98% was measured over 1500 h of aging time. Increasing temperature to 120 °C or applied load to 400 psi resulted in maximum strains of 2.0 and 1.5%, respectively. Water phase transition during freezing conditions (54 freeze–thaw cycles between −35 and 20 °C) had no effect on GDL strain. No change was observed for in-plane electrical resistivity, bending stiffness, surface contact angle, porosity and water vapor diffusion after 50 consecutive freeze–thaw cycles between −35 and 20 °C, was measured. An increase in in-plane and through-plane air permeability (18 and 80%, respectively) was attributed to material loss during permeability measurements. Ex situ tests showed that convective air flow can cause material loss, resulting in increased permeability and further convection. The GDL was shown to be much more resilient to material loss in the absence of water phase transitions.

Keywords: Fuel cell; Gas diffusion layer; Compression; Strain; Freezing; Durability

1. Introduction

In the development of polymer electrolyte membrane fuel cells (PEMFCs) for transportation applications, durability is a major challenge to fuel cell commercialisation [1]. PEMFC systems will be required to have a 5000 h lifespan and be able to maintain performance under climatic conditions ranging from −40 to 40 °C. Stack components will have to tolerate −40 °C and permit the PEMFC to start up at −20 °C.

The gas diffusion layer (GDL) serves key functions in a PEMFC [2] (Table 1). Carbon fibre products in the form of papers are typical GDL materials due to their high porosity, electrical and thermal conductivity, corrosion resistance, and mechanical strength [2]. They are usually treated with a hydrophobic polymer coating [2,3] such as polytetrafluoroethylene (PTFE) [4–6] in order to improve water removal and prevent mass transport losses due to flooding at high current densities. In addition to a bulk hydrophobic treatment, GDLs are often coated with a microporous layer (MPL) on their catalyst-facing surfaces to aid in liquid water transport [2,4,7–9] and current collection [2,4,8].

Parametric [5,10–13] and modelling [14–23] studies have shown that GDL characteristics affect overall fuel cell performance; however, the impact of GDL materials and designs on PEMFC durability is not well characterised [2]. The analysis of GDLs which have been operated in situ has not been a focal point of past PEMFC durability studies [24–34]. Conventional electrochemical operation of a cell or stack makes GDL durability a difficult area of study due to the lengthy test times required, the complexity of analysis given the various components in a membrane electrode assembly (MEA), and the overlapping of failure causes from interaction effects among MEA components [26].

Recent publications [35–37] pointed towards the use of ex situ methods in the study of GDL durability. Ex situ methods enable individual GDL ageing, without having to operate an entire stack, and remove confounding effects from adjoining components from the analysis. A decrease in sessile drop contact angle of a 17 wt% fluorinated ethylene propylene (FEP)-coated carbon fibre paper with immersion time in de-ionised water with nitrogen and air sparging, at 60 and 80 °C was reported [35]. The decrease in hydrophobicity occurred in the first 100–150 h

* Corresponding author. Permanent address: Clean Energy Research Centre, University of British Columbia, 6250 Applied Science Lane, Vancouver, B.C., Canada V6T 1Z4. Tel.: +1 604 822 4189; fax: +1 604 822 2403.
E-mail address: walter.merida@ubc.ca (W. Mérida).

0378-7753/$ – see front matter © 2006 Elsevier B.V. All rights reserved.
doi:10.1016/j.jpowsour.2006.09.092

Nomenclature

A	cross-sectional flow area [m^2]
c	concentration [$kg\,m^{-3}$]
D	diffusion coefficient in open air [$m^2\,s^{-1}$]
D_{eff}	diffusion coefficient in porous media [$m^2\,s^{-1}$]
k	permeability coefficient [m^2]
L	length [m]
δL	change in length [m]
ΔP	pressure drop [Pa]
Q	volume flow rate [$m^3\,s^{-1}$]
R	electrical resistance [Ω]
s	distance [m]
t	time [s]
δT	change in temperature [°C]
w	width [m]
x	thickness [m]
x_0	initial thickness [m]
ΔX	flow-path length [m]

Greek symbols

α	compressive strain
β	coefficient of thermal expansion [K^{-1}]
ε	porosity
μ	fluid viscosity [Pa s]
ρ	electrical resistivity [Ω m]
τ	tortuosity

of immersion time, and was greater for the air atmosphere case. Reasons for the decreased hydrophobicity were not discussed. In another study [36] GDLs were aged in 15 wt% hydrogen peroxide at 82 °C. Weight loss and MPL contact angle were monitored and found to increase with increased time of exposure, and were attributed to oxidation of the carbon in the MPL. GDLs aged up to 264 h were built into MEAs. With increased time in the peroxide bath, MEA performance showed increased losses in the mass transport portion of the polarisation curve. That was consistent with the results given for a long-term fuel cell test and showed that GDL oxidation can reduce MEA performance. The possibility that MPL carbon surface oxidation with an accompanying decrease in sessile drop contact angle could affect water transport in PEMFCs and contribute to mass transport losses has been raised elsewhere [37]. Electrochemical surface oxidation experiments consisted of submerging GDL samples in 1 M H_2SO_4 under a constant potential. After 120 h at 1.2 V (versus a reference hydrogen electrode), the contact angle of a 10 wt% PTFE-Vulcan MPL decreased from $147° \pm 3°$ to $111° \pm 7°$.

Table 1
GDL functions within a PEMFC

GDL function	Description
Reactant transport	Facilitate the transport of reactant gases between flow-field and catalyst layer
Water transport	Facilitate the transport of gaseous and liquid water between flow field and catalyst layer
Electronic conductivity	Facilitate electronic conduction between the flow field and catalyst
Thermal conductivity	Facilitate thermal conduction between the flow field and catalyst
Mechanical support	Provide mechanical support for the catalyst layer and membrane

The experimental and modelling work in the literature have shown that GDL permeability affects fuel cell beginning-of-life performance [5,11,12,38]. A change in material characteristic may affect the functional performance of a PEMFC [39]. It is plausible that if GDL permeability changes over time in an operating fuel cell, then subsequent PEMFC performance and durability could be affected. GDL in-plane permeability was shown to decrease with cell clamping pressure [11,40], and PEMFC operation showed GDLs to be susceptible to poor mass transport arising from a loss of porosity when the cell compression force was increased [10,11]. These results agree in general with modelling efforts which show a lowered porosity to be detrimental to performance [18–23]. A shift away from the parametric methods used in past studies of permeability and porosity towards time-based measurements will generate useful durability data. The possibility of a loss in mass transfer of reactants to the electrodes over time due to compressive strain from mechanical stress or damage of the GDL during operation has been raised [24] but has yet to be verified. It is not known if compressive strain of the GDL occurs as a result of fuel cell operation, but if it were to occur then performance could be negatively impacted. GDL strain should be considered in the development of PEMFCs with longer lifetimes and higher power densities.

Commercial applications will require PEMFCs to be durable under ambient temperatures down to −40 °C, and the need to characterise morphological changes and localized stresses in fuel cell components associated with water phase transition during freezing conditions has been pointed out [41]. Reduced GDL surface hydrophobicity from cold-start conditions has been observed [34] and indicates further investigation of the GDL is warranted. GDL strain may occur as a result of water phase transition during freezing conditions, and should be investigated. Although GDL properties of thickness [5,10,11], electrical resistivity [5,11,12], pore-size distribution [5,11,12], gas permeability [5,11,12], and contact angle [11,34–37] have been studied, the effect of freezing conditions on them is largely unknown.

The purpose of this work was to use ex situ methods to study GDL compressive strain under steady-state and freezing conditions, and to investigate the effect of freezing conditions on GDL electrical resistivity, bending stiffness, air permeability, surface contact angle, porosity and water vapor diffusion. The results and experimental approach of this work can be used to aid in the development of GDL materials and ensure durable PEMFC systems.

2. Experimental apparatus and procedure

2.1. Gas diffusion layer samples

A single GDL was aged under a combination of physical and environmental conditions, and properties were monitored as a function of aging time (Table 2).

Table 2
Experimental approach used in this study

Ex situ evaluation	Ex situ aging
• Compressive strain as a function of aging time and number of freeze–thaw cycles	• Physical stress from test fixture • Environmental exposure using water bath and environment chamber
• The following as functions of the number of freeze–thaw cycles: -Electrical resistivity -Bending stiffness -Air permeability -Surface contact angle -Porosity -Water vapor diffusion	• Freezing conditions using an environment chamber

The GDL used in this study was prepared using common fabrication methods [42,43], and was typical of dual-layer GDLs studied in the literature [15,42,43]. Carbon fibre paper (CFP) (TGP-H-060, Toray Industries) was treated by soaking in a PTFE dispersion (Teflon® PTFE 30B, DuPont), followed by sintering at 400 °C for 10 min in a convection oven. The resulting hydrophobic CFP (HCFP) had a PTFE loading of 6 wt%. A MPL ink was prepared by mixing acetylene black (Shawinigan® AB50 grade; Chevron), PTFE, and de-ionised water. This MPL ink was then screen printed onto the HCFP. The resulting GDL was sintered at 400 °C for 10 min in a convection oven, and had a MPL loading of 0.6 mg cm^{-2}.

GDL materials were compacted at 165 °C and 400 psi for 2 min in a heated press. This was done to expose the GDL to stresses arising from MEA manufacture. In the context of compressive strain, the hot pressing step was considered to be stressful to the GDL relative to other manufacturing operations due to the high temperatures (>100 °C) and pressures (>200 psi) typically employed [3,5,7,44–46]. GDL samples were measured with an universal testing machine (model 5569; 0.001 mm resolution; Instron Corporation) to have a thickness of 0.175 mm at 200 psi.

2.2. Test fixture for studying compressive strain

For compressive strain tests, a test fixture was developed to replicate the mechanical and physical boundary conditions found in a PEMFC, namely a compressive force, and the interaction of plate channels and landings, respectively. A fixture (Fig. 1) consisted of a stack of graphite plates sandwiched between two stainless steel end-blocks. The graphite plates had parallel flow fields (0.8 mm and 0.55 mm wide channels and landings, respectively) machined on one side with the other side flat. A piece of GDL measuring 23 mm × 30 mm was placed between each plate. A fixture accommodated seven GDL pieces. A bolt running through the end-blocks, plates and samples, together with Belleville disc springs at each end applied a compressive force to the test cell. The compressive force exerted on the GDL via the plate landings was set at 200 psi, at 20 °C, by pre-loading the disc springs with a pneumatic cylinder and then hand-tightening the nut on the bolt.

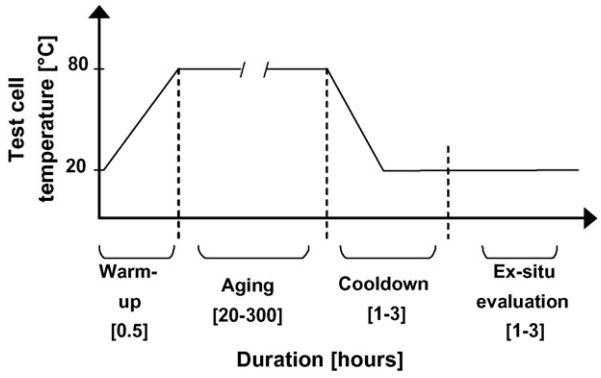

Fig. 2. Temperature–time profile used in steady-state aging of the GDL. The duration of the stages of aging are shown.

2.3. Aging procedure

2.3.1. Steady-state conditions

GDL samples assembled in test fixtures were aged in a temperature-controlled de-ionised water bath. The temperature–time profile of steady-state experiments is shown in Fig. 2. Test fixtures were introduced into the bath at a water temperature of 20 °C to prevent undue strain from large thermal gradients. The bath was then heated to the 80 °C. Aging progressed until ex situ evaluation was scheduled, at which time the fixtures were removed and air-cooled to room temperature. After ex situ evaluation, the fixtures were returned to the bath and aging proceeded as before.

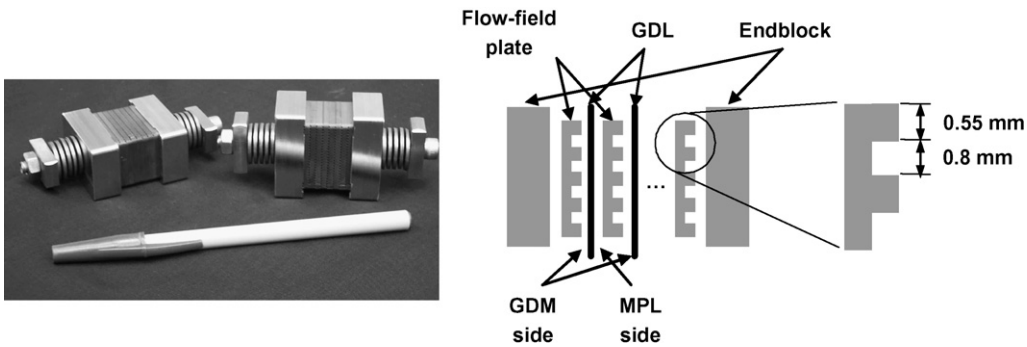

Fig. 1. Test fixtures developed to study GDL strain. Each GDL sample was placed between two flow-field plates, with the CFP side facing the channels of one plate, and the MPL side facing the back of the other plate.

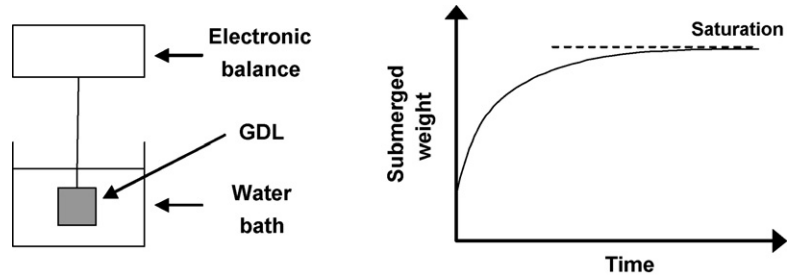

Fig. 3. Saturation of GDL samples with liquid water. Saturation was determined by monitoring the submerged weight of a sample and noting when the rate of weight gain had stabilised.

2.3.2. Freezing conditions

Prior to aging under freezing conditions, GDL samples were first saturated with liquid water to emulate the liquid water content arising from operation in a PEMFC. Saturation of GDL samples was accomplished by immersing them in a 80 °C deionised water bath, measuring their submerged weight, and noting when the rate of weight gain had decreased [47] to below 0.175 mg cm^{-2} h^{-1} (Fig. 3). Saturation resulted in water contents of 12.3–14.0 mg cm^{-2}. This was higher than the water content of 2.0 mg cm^{-2} measured in the author's lab for a GDL which had been operated under humidified conditions. The samples therefore represented an extreme-case water saturation scenario.

Saturated GDL samples for compressive strain measurements were assembled into test fixtures and placed in an automated environment chamber (ESPEC Corp; model ESZ-2CW) for aging, while samples used to investigate the effect of freezing conditions on electrical resistivity, bending stiffness, etc. were supported on a rack before being placed in the chamber. The chamber was programmed to repeatedly cycle between 20 and −35 °C at 0.3 °C min^{-1}. The minimum of −35 °C was in-line with expected requirements of PEMFC applications [41] and 20 °C was chosen to minimise any degradation which may occur at the higher temperatures typical of operation (i.e. 80 °C). The temperature–time profile used for freezing experiments is shown in Fig. 4. Aging was measured by the number of freeze–thaw cycles, with one cycle corresponding to cooling from 20 to −35 °C and heating back up to 20 °C. When ex situ evaluation was scheduled, the samples were brought up to 20 °C in the chamber and then removed. Aged GDL samples for measurements of electrical resistivity, bending stiffness, etc. were allowed to air dry before being evaluated.

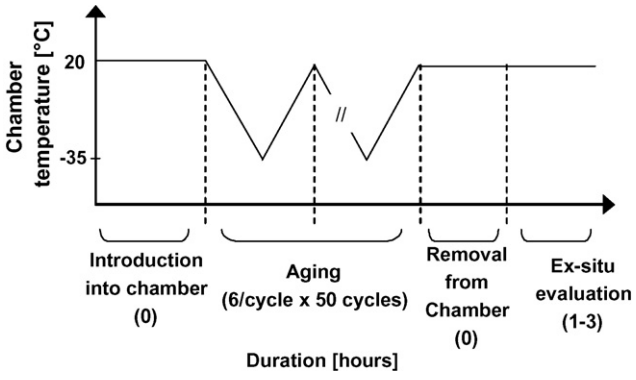

Fig. 4. Temperature–time profile used in freeze–thaw aging of the GDL. The stages of aging are shown with typical times.

2.4. Strain measurements

Thickness measurements were taken across the outer faces of the end-blocks of a test fixture with a digital micrometer (model 293-331; 0.001 mm resolution; Mitutoyo Corporation) having a 1–2 in. measurement range. Measurements were taken prior to, during and after aging, and were conducted in a climate controlled room (20.0 ± 0.5 °C). A blank test fixture with no GDL samples and assembled to 200 psi was included in measurements to account for dimensional changes of the fixture materials. Strain (α) was calculated according to

$$\alpha = \frac{x - x_0}{x_0} \times 100\% \quad (1)$$

Five thickness readings were taken at each of the four corners of the test fixture (Fig. 5), and reported thickness and strain values are the mean of 20 individual readings. The precision of the thickness measurement was ±0.0008 mm (given as $\pm 1.96\sigma$, where σ is the standard deviation of measured thickness values).

2.5. Electrical resistivity

A four-point method [2] was used to measure in-plane electrical resistivity. GDL test pieces measuring 1.3 cm × 5.5 cm were compressed under a pressure of 200 psi and a 0.1 A current was applied with an Agilent E3610A DC power supply across a set of gold-plated voltage measuring probes (each 0.7 mm wide and 1.3 cm long). The resulting voltage drop was measured with a

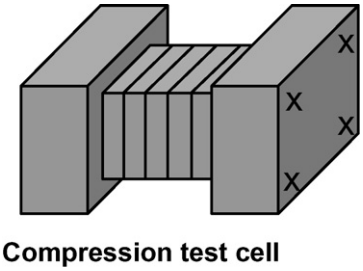

Fig. 5. Location of thickness readings (marked with an 'x') across a test fixture. Five readings were taken at each of the four corners.

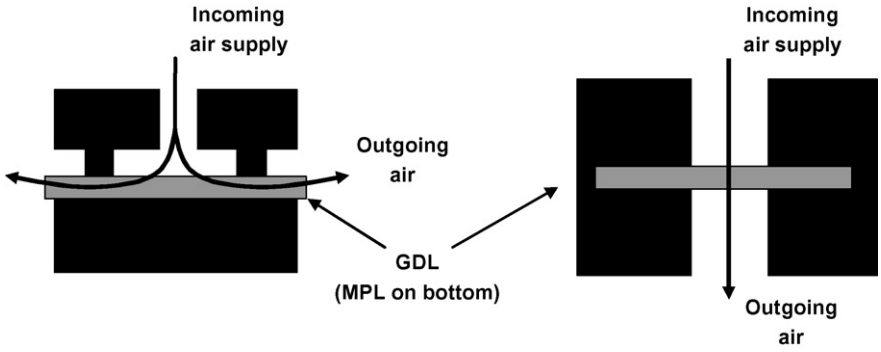

Fig. 6. Schematic of in-plane (left) and through-plane (right) air permeability measurements. Samples were tested with their catalyst-side surfaces facing down.

Fluke 87 True RMS multimeter and resistance (R) was calculated. In-plane resistivity (ρ) was calculated according to [2]

$$\rho = \frac{Rwx}{L} \tag{2}$$

where the distance between voltage probes (L) was 3 cm, the test configuration had a width (w) of 1.3 cm, and GDL thickness (x) at 200 psi was 0.175 mm.

2.6. Bending stiffness

Bending stiffness measurements were performed with a Taber Industries V-5 Model 150-E stiffness tester (Taber Industries). GDL test pieces measuring 3.8 cm × 7 cm were tested at a bend angle of 15°.

2.7. Air permeability

A Messmer Buchel Roughness tester (model no. K513; software version 3.7a; Testing Machines Inc.) was used to measure air permeability in the in- and through-plane directions (Fig. 6). The pressure drop (ΔP) across a GDL test piece as a function of flow (Q) of dry air (21 °C) was measured and permeability coefficients (k) were calculated from Darcy's law [2,11,12,48]:

$$k = \frac{Q}{A}\mu\frac{\Delta X}{\Delta P} \tag{3}$$

The fluid viscosity (μ) for dry air at 21 °C is 1.77×10^{-5} Pa s [49].

2.8. Surface contact angle

Surface contact angles were measured using the sessile drop method [2]. Fifteen-microlitre water drops were imaged with a charge-coupled device (CCD) camera (model VCB-3512T; Sanyo Electric Co., Ltd.), and contact angles were obtained from the captured images using First Ten Angstroms FTA200 software (v 1.961; Folio Instruments Inc.).

2.9. Porosity

Porosity of GDL samples were measured with an AutoPore III mercury intrusion porosimeter (software version 2.00; Micromeritics Instrument Corp.). The amount of mercury that penetrated the GDL pores was measured as a function of applied pressure.

2.10. Water vapor diffusion

Water vapor diffusion was measured using an in-house apparatus (Fig. 7). Two chambers separated by GDL test pieces were purged with dry air to remove traces of moisture. A test consisted of closing off the purge loops, introducing liquid water into the wet chamber and measuring the increase in water vapor in the dry chamber as a function of time. Measurements were made with a Testo 400 RH meter (software version 1.30; Testo Inc.) and humidity sensor (part number 0628 0008; Testo Inc.). Data from the test was fit to a time dependent one-dimensional diffusion model based on Fick's Second Law to determine the relative water vapor diffusion coefficient, given as D_{eff}/D where D_{eff} is the diffusion coefficient of water vapor through the GDL and D is that through open air:

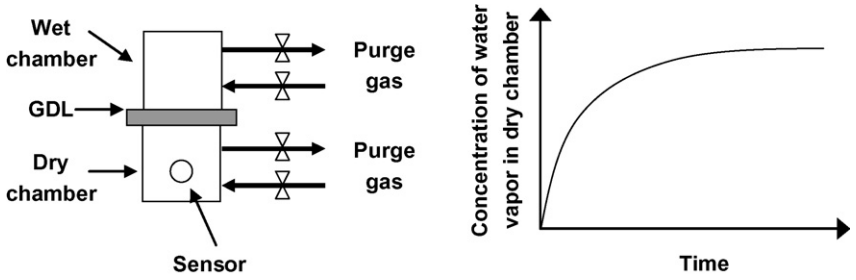

Fig. 7. Experimental setup used to measure water vapor diffusion. GDL samples were tested in the through-plane direction.

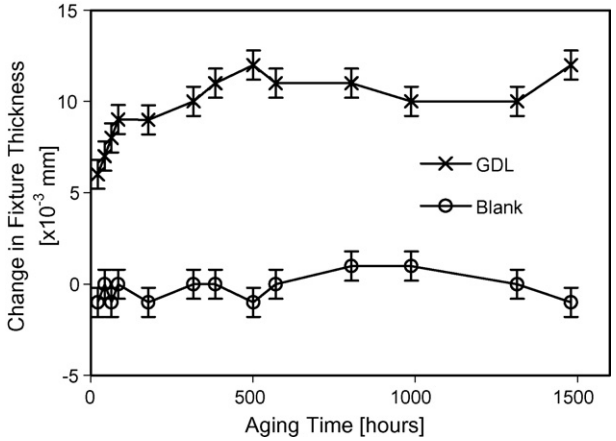

Fig. 8. Change in thickness as a function of aging time in an 80 °C water bath for GDL (with GDL samples) and blank (no GDL samples) test fixtures. Positive values correspond to shortening of the fixture. Error bars represent the precision of thickness measurements.

Dry chamber:

$$\frac{\delta c}{\delta t} = D\frac{\delta^2 c}{\delta s^2} \tag{4}$$

Sample:

$$\frac{\delta c}{\delta t} = D_{\text{eff}}\frac{\delta^2 c}{\delta s^2} \tag{5}$$

For a completely open GDL structure, D_{eff}/D is unity. All tests were done at 21 °C.

3. Results and discussion

3.1. Strain under steady-state conditions

Results of thickness measurements on test fixtures aged at 80 °C are reported in Fig. 8. The GDL test fixture dimensions decreased with aging time, and by 100 h it was 0.009 mm shorter. This continued to about 500 h, after which there was no further significant change in thickness for the remaining 1000 h of the experiment. The rate of change in thickness was greatest at the onset of aging. Results for a blank test fixture (no GDL samples) aged under identical conditions did not show an upward or downward trend, so changes in thickness were attributed to the GDL samples.

The data was re-calculated as GDL compressive strain, and is shown in Fig. 9 with additional measurements from replicate test fixtures. The data showed strain initiated at the onset of aging, and had roughly peaked by 400 h. This suggested that the GDL was experiencing an increase in compression resistance – deformation became more difficult as the GDL was strained – as aging progressed. The average maximum strain measured across test fixtures was roughly 0.98%. The variation in maximum strain values between test fixtures, between 0.82 and 1.2%, was likely a result of material variation in the GDL samples. GDL strain may be affected by area weight, density, and compositional differences within its structure.

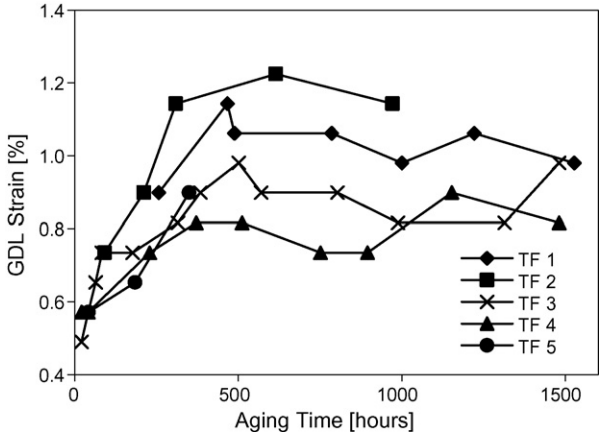

Fig. 9. GDL compressive strain as a function of aging time at 80 °C and 200 psi for samples tested in test fixtures (TF).

The results above demonstrate that GDL strain can occur over time. This should not be confused with the elastic deformation of GDL samples upon assembly in a test fixture, which occurs instantaneously, invariant of time and is fully recoverable. The strain arising from aging over time was in addition to this elastic deformation.

It is worthwhile to understand how GDL compression is affected by temperature and applied load since PEMFCs may be operated at temperatures between 80 and 120 °C [41] and cell clamping loads above 200 psi have been used [10,11].

3.1.1. Effect of temperature

Fig. 10 shows results for fixtures aged at 21 and 120 °C, under 200 psi. Previous results at 80 °C and 200 psi are included for comparison. Room temperature aging was done in a water bath, while elevated temperature aging was accomplished with an oven. A humid environment was not simulated in the oven due to the elevated temperature; however, this was not expected to affect compression in relation to temperature and applied load. The GDL was relatively stable at room temperature with strain detected at about 400 h, and not exceeding 0.16% through 971 h. Aging at 120 °C resulted in markedly increased strain, reaching

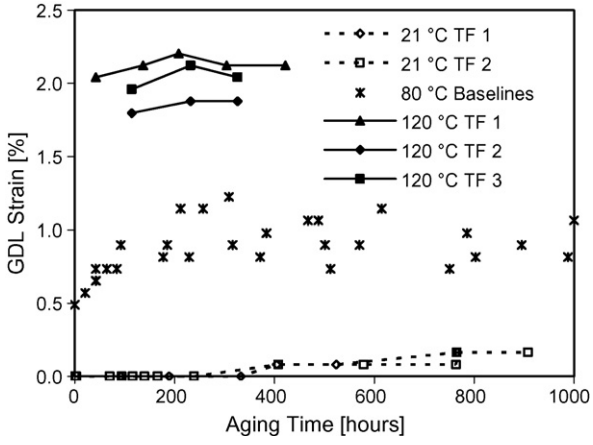

Fig. 10. GDL strain as a function of aging time at 21 and 120 °C, respectively, and 200 psi. Baseline data at 80 °C is included for comparison.

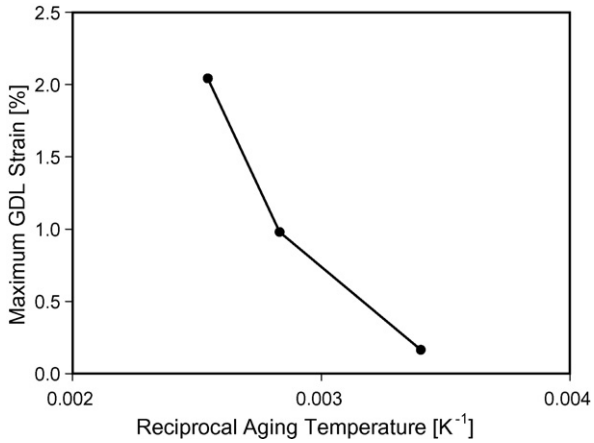

Fig. 11. Maximum GDL compressive strain as a function of reciprocal aging temperature. All data at 200 psi.

a maximum of about 2.0% by about 200 h. Comparison of results at 80 and 120 °C revealed that strain levelled off sooner at the higher temperature. A plot of maximum strain versus reciprocal aging temperature is given in Fig. 11.

3.1.2. Effect of applied load

Fig. 12 shows results for test fixtures aged under 300 and 400 psi, at 80 °C. Previous results at 200 psi and 80 °C are included for comparison. Both of the higher fixture loads resulted in increased strain. The strain levelled off at a maximum of 1.4 and 1.5% at 300 and 400 psi, respectively. A plot of maximum strain versus applied load is shown in Fig. 13.

3.2. Strain under freeze–thaw conditions

Results of thickness measurements for test fixtures aged under freezing conditions are shown in Fig. 14. After 10 freeze–thaw cycles, the fixture had shortened by 0.002 mm relative to its starting thickness. There was no further compression for an additional 10 cycles. A blank (no GDL samples) fixture aged in a similar fashion did not exhibit a net change in thickness, as a result changes in thickness were attributed to strain of the GDL.

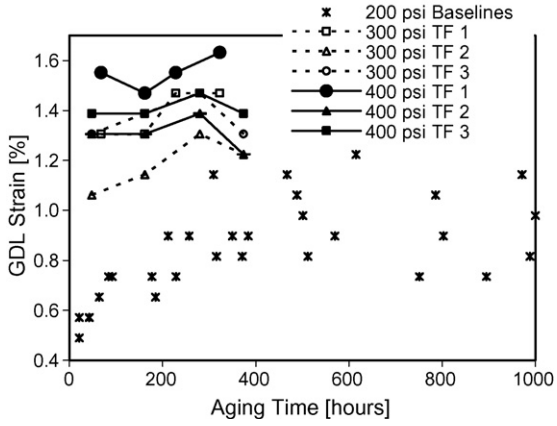

Fig. 12. GDL strain for test fixtures aged under applied loads of 300 and 400 psi, respectively. Baseline data at 200 psi is included for comparison.

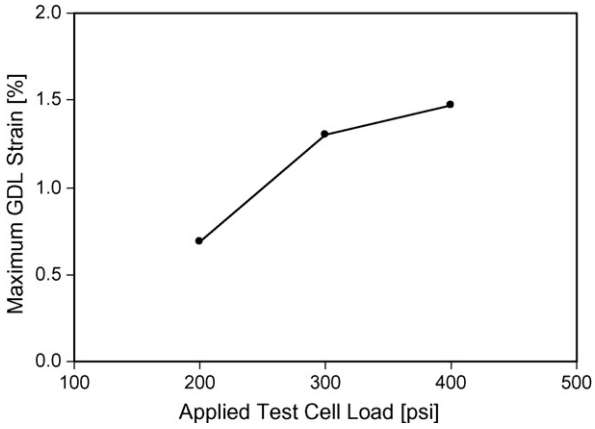

Fig. 13. Maximum GDL strain as a function of applied load. All data at 80 °C.

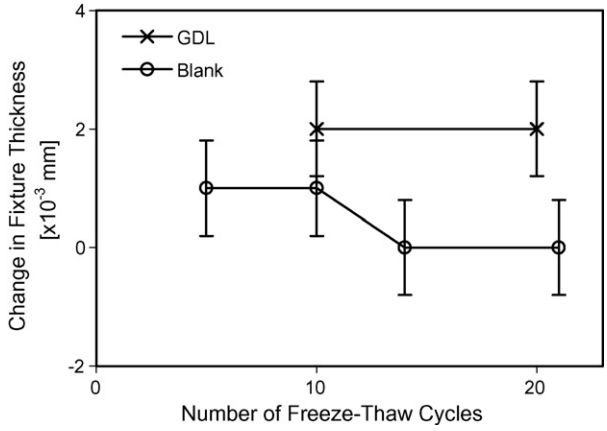

Fig. 14. Change in thickness as a function of the number of cycles between −35 and 20 °C for GDL (with GDL samples) and blank (no GDL samples) test fixtures. Positive values correspond to shortening of the fixture. The error bars represent the precision of thickness measurements.

The data was re-calculated as GDL compressive strain, and is shown in Fig. 15 with additional measurements from replicate test fixtures. Results for fixtures 1 through 4 demonstrated that strain was stable with the progression of aging cycle. The maximum amount of strain across fixtures was roughly 0.33%.

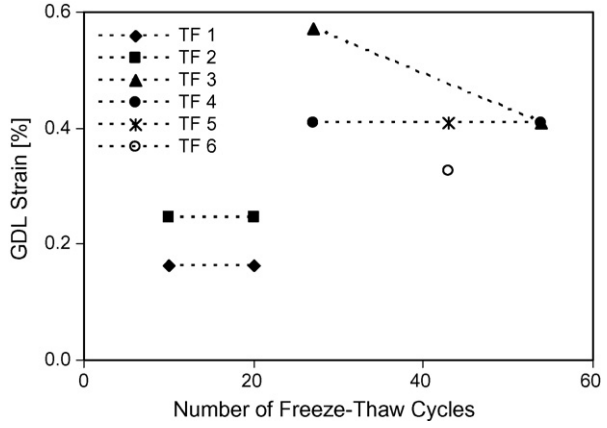

Fig. 15. GDL compressive strain as a function of freeze–thaw aging cycle number for samples tested in test fixtures (TF).

Table 3
Effect of freezing conditions through 50 consecutive cycles on GDL properties

Property	Unit	Aged GDL	Un-aged GDL	Effect
In-plane electrical resistivity	Ω cm	0.0070 ± 0.0005	0.0071 ± 0.0005	No change
Bending stiffness	Taber	34 ± 9	34 ± 6	No change
Plate-side surface contact angle	°	154 ± 13	152 ± 10	No change
Catalyst-side surface contact angle	°	159 ± 7	158 ± 6	No change
Porosity	%	76 ± 2	75 ± 2	No change
Water vapor diffusion (relative to that in open space)	–	0.216 ± 0.023	0.203 ± 0.022	No change
In-plane air permeability	$\times 10^{-13}$ m^2	2.89 ± 0.36	2.44 ± 0.33	Increase
Through-plane air permeability	$\times 10^{-13}$ m^2	8.22 ± 2.73	4.56 ± 2.46	Increase

Errors are $\pm 1.96\sigma$, where σ is the standard deviation of the measured data.

Material variation in the GDL samples and natural variation in the aging process likely resulted in the differences between fixtures. The data showed that strain was confined to a level below 0.33% through 54 freeze–thaw cycles. A greater number of freeze–thaw cycles was not tested in this study. It is not believed that further cycles would result in greater compression because of the stability exhibited by the data.

The effect due to the volume expansion of water upon freezing was tested by aging GDL samples which did not undergo the water saturation procedure discussed in Section 2.3.2. Fig. 16 shows data for samples aged in the absence of water saturation, together with previous saturated-case results. Through 43 freeze–thaw cycles, dry (GDL samples un-saturated) test fixtures exhibited strains of 0.24–0.33%. The strain was likely due to mechanical expansion–contraction of the test cells from the 55 °C differential of a freeze–thaw cycle as no liquid water was present. The linear coefficient of thermal expansion (β) of 316 stainless steel and graphite are 1.59×10^{-5} and 2.0×10^{-5} K^{-1}, respectively. Given the length (L) of the end-blocks (2 mm × 12.2 mm) and graphite plates (8 mm × 2.7 mm) in a test cell, a ±1 °C change results in a length change (δL) of ±0.82 μm according to [50]:

$$\delta L = L\beta\delta T \tag{6}$$

Cooling from room temperature causes the graphite plates to shrink more than the bolt, and the opposite happens with heating. Future work would need to look at minimising this temperature differential. For example, cycling between −2 and 2 °C with adequate dwell times at each end point would reduce the temperature differential to 4 °C and still allow sufficient time for the test cell to fully freeze and thaw.

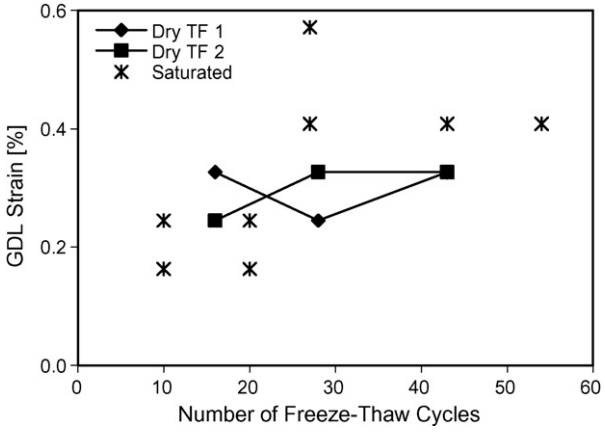

Fig. 16. Effect of water on GDL strain from freeze–thaw aging.

The similarity of the results between dry and saturated samples points to water phase transition during freezing conditions having no effect on GDL strain.

3.3. Effect of freezing conditions

The effect of freezing conditions through 50 consecutive cycles between −35 and 20 °C on GDL electrical resistivity, bending stiffness, air permeability, surface contact angle, porosity and water vapor diffusion is shown in Table 3.

In-plane electrical resistivity was not affected by aging under freezing conditions (Table 3). In-plane conductivity is necessary for effective utilisation of the catalyst layer out over channels [2]. An increase in resistivity would negatively impact the GDL's function as a current collector between the flow field and catalyst layer, and increase ohmic losses [51].

Bending stiffness was not altered as a result of aging (Table 3). A compromised bending stiffness may affect the GDL's ability to mechanically support the catalyst and membrane over channel areas. Reduced flexural strength may lead to intrusion of the GDL into the channels and cause reactant flow-field pressure drop to increase, resulting in higher compressor power requirements and negatively impacting system efficiency [20].

Surface contact angles of plate-side and catalyst-side surfaces were not altered by freezing conditions (Table 3). The measured values are in the range of those reported for the plate-side [51] and catalyst-side [52] surfaces, respectively. This contradicts the results of Oszcipok et al. [34] who reported an increase in surface wetting of both plate- and catalyst-side surfaces of a cathode GDL operated through 10 cold-start experiments from −10 °C. It is not known what the reason for their increase was, but increased wetting of the GDL can arise from changes in the surface chemistry of fibres [24,53], PTFE loss [24,53], PTFE degradation [25] or contaminants [54].

Water vapor diffusion data showed that aging under freezing conditions did not change the GDL's ability to transport water vapor (Table 3). The diffusion of water vapor across the GDL is roughly 20% of that in open space. The effective diffusion coefficient of a porous medium is given by [12]

$$D_{\text{eff}} = \frac{\varepsilon}{\tau} D \tag{7}$$

Table 4
Effect of water phase transition on GDL air permeability

Property	Dry-aged GDL	Un-aged GDL
In-plane air permeability [$\times 10^{-13}$ m^2]	2.53 ± 0.36	2.44 ± 0.33
Through-plane air permeability [$\times 10^{-13}$ m^2]	5.14 ± 2.72	4.56 ± 2.46

Errors are $\pm 1.96\sigma$, where σ is the standard deviation of the measured data.

Table 5
Effect of through-plane permeability measurement on GDL sample weight

	Aged GDL	Un-aged GDL
Weight loss [mg]	0.28	0.05

The water vapor diffusion reported in Table 3 is effectively $D_{\text{eff}}/D = \varepsilon/\tau$. Bulk porosity ($\varepsilon$) was not altered by water phase transition through 50 cycles (Table 3). Given the results for porosity and water vapor diffusion, it follows that tortuosity (τ) must have been unchanged as well.

3.3.1. Change in air permeability

In- and through-plane air permeabilities were measured to increase 18 and 80%, respectively (Table 3). The effect of volume expansion of water upon freezing was tested by aging GDL samples which did not undergo the water saturation procedure discussed in Section 2.3.2. Table 4 shows air permeability data for dry-aged samples. Through 50 freeze–thaw cycles, air permeability was not altered. Temperature cycles alone did not affect permeability and it follows that the measured increase in Table 3 was due to water phase transition during freezing conditions.

The result that air permeability increased could not be explained by a change in porosity from aging, as there was none measured. Weight measurements revealed that samples experienced a loss in weight as a result of through-plane permeability measurements (Table 5). Visual analysis of material collected at the outlet of the permeability setup showed this weight loss to be due to material loss from the GDL. Fig. 17 shows a magnified picture of the material collected, which was comprised of the MPL (dark material in picture). Carbon fibres which come across much brighter than the MPL in pictures were not found in the outlet stream.

Table 6 shows that the addition of a MPL to a PTFE-treated carbon fibre paper (HCFP) decreased in-plane permeability by 62% and through-plane permeability by 87%. This reduction in air permeability is in agreement with the works of others [11,12],

Table 6
Effect of MPL addition on air permeability

	Un-aged GDL	Un-aged HCFP
In-plane air permeability [$\times 10^{-13}$ m^2]	2.44 ± 0.35	6.37 ± 0.35
Through-plane air permeability [$\times 10^{-13}$ m^2]	4.56 ± 2.46	34.3 ± 5.05

Errors are $\pm 1.96\sigma$, where σ is the standard deviation of the measured data.

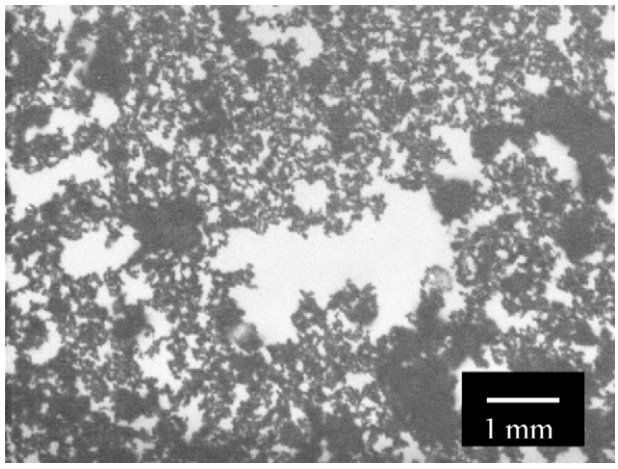

Fig. 17. Optical micrograph of MPL material dislodged from aged GDL samples during through-plane permeability measurements.

and is a result of the smaller pore size of the MPL (0.01–10 μm) compared to that for the HCFP (10–100 μm) (Fig. 18). The reduction in air permeability is greatest in the through-plane direction as the MPL is placed in series with the HCFP [15]. Loss of MPL material would lead to decreased air flow resistance and a higher permeability. It is likely that MPL material loss during permeability measurement was the cause of the increased through-plane permeability reported in Table 3. This result is expected to extend to the in-plane orientation as MPL addition affected in-plane permeability (Table 6), although to a lesser extent than in the through-plane configuration. Even though water phase transition during aging did not cause a measurable change in porosity, it is believed to have sufficiently weakened the MPL such that subsequent air flow from air permeability measurements resulted in a loss of material. This result demonstrates that the GDL can be affected by water phase transition during freezing.

The following reason for why a structurally weakened MPL was not detected in aged samples by other ex situ measures is offered: those measures either did not strongly affect the MPL or were not strongly affected by the MPL. For example, water vapor diffusion measurements did not affect the MPL structure (by removing material) as diffusion of water vapor was

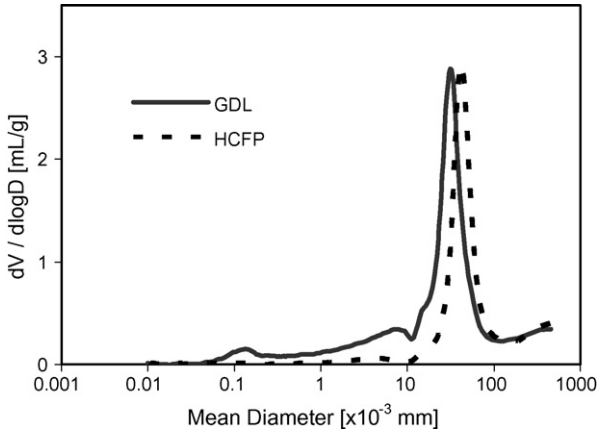

Fig. 18. Measured pore-size distribution of un-aged HCFP and GDL samples.

Table 7
Effect of MPL addition on the bending stiffness of PTFE-treated carbon fibre paper

	Un-aged GDL	Un-aged HCFP
Bending stiffness [Taber]	34 ± 5	33 ± 2

benign, whereas permeability measurements involved bulk air flow which disturbed the weakened MPL. In the case of bending stiffness, MPL addition had no effect on bending stiffness values (Table 7), so a weakened MPL structure was not detected.

3.3.2. Effect of in-plane air flow

Convective air flow in a PEMFC in the through-plane orientation across the GDL is not a possibility due to the cell geometry. GDL in-plane flow in a PEMFC however has been studied experimentally [38] and modelled [14–17]. As such, MPL structural integrity and material loss was investigated further in the in-plane configuration.

Fig. 19 shows results for un-aged GDL samples tested in the in-plane orientation at different pressure differential levels, with new samples tested at each level. The flow rate necessary to maintain a given pressure differential as a function of time was measured to permit the dynamics of material loss to be studied. The time measured from the onset of air flow is given on the horizontal axis, and the vertical axis reports the in-plane permeability of the sample relative to its initial permeability when air flow had just initiated. At a pressure differential of 1.47 kPa, the un-aged sample was stable over time and did not vary from its initial value at the onset of air flow. At 6.89 kPa, permeability increased with time and reached a plateau value 1.007 times that at the start after roughly 3 min. Results for 27.6 kPa were similar. At 68.9 kPa, permeability was still increasing after 5 min of air flow, beyond a value 1.035 times that at the start. The rate of increase was greatest at the onset of air flow and decreased monotonically with time.

As pressure drop remained constant, increasing flow rate with time could be due to MPL material loss. This was not confirmed as the in-plane experimental setup was not conducive to outlet stream capture, and weight measurements of the GDL samples did not reveal a detectable change in mass. This latter point was not surprising given the small change in permeability which was observed: an increase of just 1.035 times at a pressure differential of 68.9 kPa. The weight loss reported in Section 3.3.1 was detected in conjunction with a 1.8 times increase in through-plane permeability (from 4.56×10^{-13} to 8.22×10^{-13} m^2).

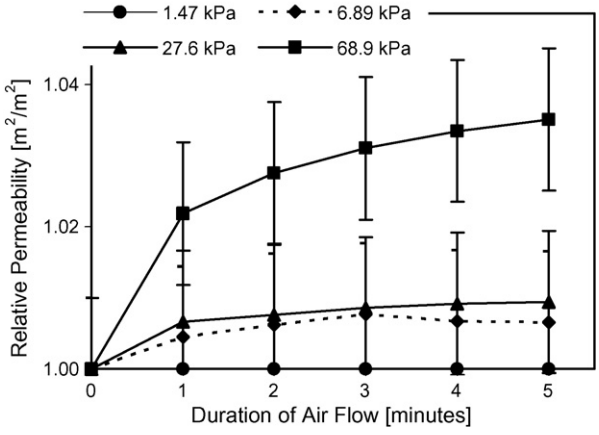

Fig. 19. Measured change in in-plane permeability as a function of time under air flow necessary to maintain a given pressure differential across an un-aged GDL sample. Error bars are $\pm 1.96\sigma$, where σ is the standard deviation of the measured data.

Aged GDL samples were also tested in-plane; however, the rate of increase in permeability was several times greater than that shown in Fig. 19. This did not permit reliable experimental measurements to be made at the onset of air flow, and an analysis of the dynamics involved was not possible. Instead, in-plane permeability results from Table 3 were considered. At a pressure differential of 1.47 kPa, aged samples were assumed to have a starting permeability of 2.44×10^{-13} m^2, the same as that for un-aged samples. Aged and un-aged samples were considered to have the same permeability at the onset of air flow as material loss had yet to occur. With air flow, permeability of aged samples reached a plateau of 2.89×10^{-13} m^2, 1.18 times their initial value. This is roughly 14% greater than the largest change (1.035 times at a pressure differential of 68.9 kPa) measured in Fig. 19. This shows that the structural integrity of the MPL can be significantly compromised by freezing conditions, while in the absence of water phase transitions, the MPL is much more resilient to changes in air permeability.

3.4. Discussion

3.4.1. Effect of compressive strain on channel pressure drop

Impingement of the GDL into the channels of the flow-field [11,16,55] can result in increased pressure drop and decreased system efficiency during operation as compressors and pumps compensate for reduced reactant flow [2,56]. A MEA utilising the GDL under study was assembled in a single cell stack with plates of the same material and flow-field used in aging experiments. Dry air was flowed through the single cell with the channel pressure drop between inlet and outlet tracked as the applied load on the MEA was increased from 200 to 248 psi to cause a 1.7 μm elastic deformation of the GDL. A 2.5% increase in pressure drop of the single cell was measured.

It was not known to what degree the compressive strain measured in this study was manifested as channel impingement. If the effect of GDL strain can be modelled elastically, i.e. a 1.7 μm thickness change from aging over time under a constant load is the same as a 1.7 μm elastic deformation arising from an increase in applied load, pressure drop is estimated to increase 2.5%. Further experimentation in situ is needed to understand the effect of GDL strain on channel pressure drop.

3.4.2. Effect of compressive strain on air permeability

A 0.98% strain did not result in a shift in in-plane and through-plane air permeability coefficients, respectively (Table 8). Intuitively, a decrease in air permeability due to the reduced porosity of a GDL having undergone compressive strain was expected.

Table 8
Comparison of air permeability of aged and un-aged GDL samples

Material	In-plane permeability coefficient $\pm\sigma$ [$\times 10^{-12}$ m^2]	Through-plane permeability coefficient $\pm\sigma$ [$\times 10^{-13}$ m^2]
Aged GDL	2.42 ± 0.31	6.13 ± 1.32
Un-aged GDL	2.42 ± 0.22	6.11 ± 1.11

Measurements were done under a clamping pressure of 200 psi.

Given the small amount of strain, the expected effect was likely too small to be detected. In-plane permeability values in Table 8 are different from those in Table 3 as a result of the test head used (Fig. 6). The in-plane test head had the same landing design as a test fixture for compressive strain tests, namely a landing width of 0.55 mm, whereas permeability values in Table 3 were obtained using a general test head with a 2.0 mm landing width. Permeability values calculated from Eq. (3) should be independent of landing width (ΔX), and the above unexpected interaction effect between GDL and landing width will need to be resolved with further work. Discussions to this point have been comparative and remain unaffected.

In-plane air permeabilities of GDLs ranging from 2.3×10^{-13} to 1.4×10^{-12} m^2 under 200 psi clamping pressure have been reported [11], and are in agreement with those in Table 8 (and Table 3). Cell clamping pressure has been shown to decrease GDL air permeability [11,17,40] which impacted negatively on fuel cell performance [10,11]. A 69% reduction in in-plane permeability from 3.6×10^{-12} to 1.1×10^{-12} m^2 resulted in a 5% cell voltage decrease at 1 A cm^{-2} [11]. Measurements of in-plane air permeability and sample thickness as a function of applied compressive load resulted in the permeability-thickness relation shown in Fig. 20. As the applied load on a GDL sample is increased, elastic deformation of the GDL resulted in a thinner sample which was less permeable. This was consistent with the results reported in other studies [11,17,40].

If the effect of GDL strain can be modelled elastically (an assumption that needs to be verified with further time-based experimentation), a 1.7 μm decrease in thickness from a nominal value of 175 μm decreases in-plane permeability by 14% according to Fig. 20. For comparison, a 69% reduction in in-plane permeability from a nominal value of 2.42×10^{-12} to 0.75×10^{-13} m^2 would require a 15 μm decrease in thickness. Future work will need to look at the effect of GDL strain on air permeability and PEMFC performance.

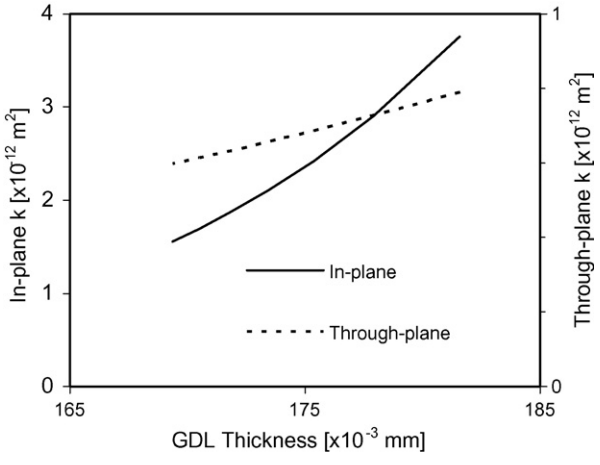

Fig. 20. Measured relation between air permeability and thickness under an applied load for un-aged GDL.

3.4.3. Flow-sharing and convection

Reactant bypass through the GDL from one channel to another has been modelled [14–17], and studied experimentally [57]. Results have been mixed: flow-sharing has been found to lower performance due to poor reactant usage [17], but others have reported that cathode performance benefited in the vicinity of the bypass [16,38]. Irrespective of these competing results, it is clear that increased permeability increases the likelihood of reactant bypass [57]. Permeabilities in the range 1×10^{-15} to 2.3×10^{-11} m^2 [16] and 10^{-14} to 10^{-8} m^2 [15] have been modelled, with flow-sharing becoming important as in-plane permeability increased above 1×10^{-13} m^2 [15]. The in-plane permeability of the GDL in this study (Tables 3 and 8) is above this threshold value, meaning flow-sharing may be possible and the effect of convection on fuel cell performance cannot be discounted.

GDL strain has the possible effect of decreasing in-plane permeability, thereby reducing flow-sharing over time. If a starting GDL experiences flow cross-over, compressive strain could lower its in-plane permeability at landing areas, and reduce reactant bypass. Reducing flow-sharing with a reduction in landing area porosity has been discussed [57].

What is more, an experimental study [38] reported convection in a GDL having a through-plane permeability of 7.5×10^{-14} m^2. Again, the through-plane permeability of the GDL in this study (Tables 3 and 8) exceeds this threshold value. Given this, the onset of convection cannot be discounted. Our results showed that convective air flow can cause material loss, resulting in increased permeability and further convection. It is not known if this extends to a PEMFC and will need to be verified with further testing in situ.

3.4.4. Material loss

Since the MPL forms part of a GDL, MPL material loss may possibly compromise GDL function and PEMFC performance. The MPL is necessary for effective current collection [2,4,8] and water management [2,4,7–9]. MPL material loss from within the GDL may impact current collection and water management. The GDL's ability to provide mechanical support to the catalyst layer and membrane may also be affected. Further experimentation is required to study these effects.

4. Conclusions

This work reported the results of an investigation of (i) gas diffusion layer compressive strain under steady-state and freezing conditions, and (ii) the effect of freezing conditions on GDL properties of electrical resistivity, bending stiffness, air permeability, surface contact angle, porosity and water vapor diffusion. An ex situ experimental approach permitted the GDL to be evaluated as a function of aging time.

Table 9
Maximum GDL strain (%) achieved during steady-state aging

Test fixture load [psi]	Aging temperature [°C]		
	21	80	120
200	0.16	0.98	2.0
300	–	1.4	–
400	–	1.5	–

GDL compressive strain occurred under steady-state conditions of 80 °C and 200 psi. A maximum strain of 0.98% was measured over 1500 h of aging time. The effect of temperature and applied load on GDL strain is summarised in Table 9. Increasing temperature to 120 °C or applied load to 400 psi resulted in maximum strains of 2.0 and 1.5%, respectively. Temperature had a larger effect on maximum strain than fixture load, over the range of aging conditions employed. This strong thermal dependence implied that GDL strain was influenced by the PTFE within the GDL. The mechanical properties of PTFE are known to be dependent on temperature [58,59]. The carbon fibres of the CFP and the carbon black of the MPL were considered to be thermally stable relative to the PTFE under the temperatures considered. Further work on GDL strain should include aging of CFP and HCFP materials to study the effect of PTFE on strain. Water phase transition during freezing conditions (54 freeze–thaw cycles between −35 and 20 °C) had no effect on GDL strain. As no previous studies on GDL compressive strain have been reported, these results provide a point of reference in the study of GDL durability. Further exploration in situ is essential to understanding the impact on operation and performance.

No change in in-plane electrical resistivity, bending stiffness, surface contact angle, porosity and water vapor diffusion, through 50 consecutive freeze–thaw cycles between −35 and 20 °C, was measured. An increase in in-plane and through-plane air permeability (18 and 80%, respectively) was attributed to material loss during permeability measurements. It was believed that aging under freezing conditions weakened the MPL structurally such that it was prone to material loss from air flow through the GDL. Indeed, ex situ tests showed that convective air flow can cause material loss, resulting in increased permeability and further convection. It is not known if these results extend to the PEMFC and further testing in situ is needed. The GDL was shown to be much more resilient to changes in air permeability in the absence of water phase transitions.

Acknowledgements

The authors would like to acknowledge the Natural Sciences and Engineering Research Council of Canada for their funding of this work.

References

[1] United States of America Department of Energy Fuel Cell Report to Congress (ESECS EE 1973), February 2003.
[2] M.F. Mathias, J. Roth, J. Fleming, W. Lehnert, in: W. Vielstich, H. Gasteiger, A. Lamm (Eds.), Handbook of Fuel Cells: Fundamentals, Technology and Applications, vol. 3, Wiley, 2003, pp. 525–534.
[3] C. Lim, C. Wang, Electrochim. Acta 49 (2004) 4149–4156.
[4] G.G. Park, Y.J. Sohn, T.H. Yang, Y.G. Yoon, W.Y. Lee, C.S. Kim, J. Power Sources 131 (2004) 182–187.
[5] M. Prasanna, H.Y. Ha, E.A. Cho, S.A. Hong, I.H. Oh, J. Power Sources 131 (2004) 147–154.
[6] T. Frey, M. Linardi, Electrochim. Acta 50 (2004) 99–105.
[7] J. Mirzazadeh, E. Saievar-Iranizad, L. Nahavandi, J. Power Sources 131 (2004) 194–199.
[8] Z. Qui, A. Kaufman, J. Power Sources 109 (2002) 38–46.
[9] F. Lufrano, E. Passalacqua, G. Squadrito, A. Patti, L. Giorgo, J. Appl. Electrochem. 29 (1999) 445–448.
[10] W.K. Lee, C.H. Ho, J.W.V. Zee, M. Murthy, J. Power Sources 84 (1999) 45–51.
[11] J. Ihonen, M. Mikkola, G. Lindbergh, J. Electrochem. Soc. 151 (2004) 1152–1161.
[12] M.V. Williams, E. Begg, L. Bonville, H.R. Kunz, J.M. Fenton, J. Electrochem. Soc. 151 (2004) 1173–1180.
[13] H.-K. Lee, J.-H. Park, D.-Y. Kim, T.-H. Lee, J. Power Sources 131 (2004) 200–206.
[14] P.H. Oosthuizen, L. Sun, K.B. McAuley, Appl. Therm. Eng. 25 (2005) 1083–1096.
[15] J.G. Pharoah, J. Power Sources 144 (2005) 77–82.
[16] W. Sun, B.A. Peppley, K. Karan, J. Power Sources 144 (2005) 42–53.
[17] H. Dohle, R. Hung, N. Kimiaie, J. Mergel, M. Muller, J. Power Sources 124 (2003) 371–384.
[18] J.H. Nam, M. Kaviany, Int. J. Heat Mass Transfer 46 (2003) 4595–4611.
[19] H.S. Chu, C. Yeh, F. Chen, J. Power Sources 123 (2003) 1–9.
[20] U. Pasaogullari, C.Y. Wang, J. Electrochem. Soc. 151 (2004) 399–406.
[21] T. Berning, Three-dimensional Computational Analysis of Transport Phenomena in a PEM Fuel Cell, University of Victoria, 2002.
[22] K.T. Jeng, S.F. Lee, G.F. Tsai, C.H. Wang, J. Power Sources 138 (2004) 41–50.
[23] W.M. Yan, C.Y. Soong, F. Chen, H.S. Chu, J. Power Sources 125 (2004) 27–39.
[24] M.W. Fowler, Degradation and Reliability Modeling of Polymer Electrolyte Membrane (PEM) Fuel Cells, Royal Military College of Canada, 2002.
[25] E. Gulzow, M. Schulze, N. Wagner, T. Kaz, R. Reissner, G. Steinhilber, A. Schneider, J. Power Sources 86 (2000) 352–362.
[26] J. Xie, D.L. Wood, D.M. Wayne, T.A. Zawodzinski, P. Atanassov, R.L. Borup, J. Electrochem. Soc. 152 (2005) 104–113.
[27] S.-Y. Ahn, S.-J. Shin, H.Y. Ha, S.-A. Hong, Y.-C. Lee, T.W. Lim, I.-H. Oh, J. Power Sources 106 (2002) 295–303.
[28] M. Betournay, G. Bonnell, E. Edwardson, D. Paktunc, A. Kaufman, A. Lomma, J. Power Sources 134 (2004) 80–87.
[29] S.D. Knights, K.M. Colbow, J. St-Pierre, D.P. Wilkinson, J. Power Sources 127 (2004) 127–134.
[30] M.S. Wilson, J.A. Valerio, S. Gottesfeld, Electrochim. Acta 40 (1995) 355–363.
[31] E.A. Cho, J.J. Ko, H.Y. Ha, S.A. Hong, K.Y. Lee, T.W. Lim, I.H. Oh, J. Electrochem. Soc. 150 (2003) 1667–1670.
[32] E.A. Cho, J.J. Ko, H.Y. Ha, S.A. Hong, K.Y. Lee, T.W. Lim, I.H. Oh, J. Electrochem. Soc. 151 (2004) 661–665.
[33] Y. Hishinuma, T. Chikahisa, F. Kagami, T. Ogawa, JSME Int. J. 47 (2004) 235–241.
[34] M. Oszcipok, D. Riemann, U. Kronenwett, M. Kreideweis, M. Zedda, J. Power Sources 145 (2005) 407–415.
[35] D.L. Wood, J. Xie, S.D. Pacheco, J.R. Davey, R.L. Borup, F. Garzon, P. Atanassov, 2004 Fuel Cell Seminar, San Antonio, TX, November 2004, 2004.
[36] J. Frisk, M. Hicks, A.T. Radoslav, W.M. Boand, A.K. Schmoeckel, M.J. Kurkowski, 2004 Fuel Cell Seminar, San Antonio, TX, November 2004, 2004.
[37] K.H. Kangasniemi, D.A. Condit, T.D. Jarvi, J. Electrochem. Soc. 151 (2004) 125–132.
[38] M.V. Williams, H.R. Kunz, J.M. Fenton, J. Electrochem. Soc. 151 (2004) 1617–1627.
[39] K. Reifsnider, X. Huang, G. Ju, M. Feshler, K. An, Mech. Comp. Mater. 41 (2005) 1–8.

[40] W.-K. Lee, J.W.V. Zee, A. Jena, K. Gupta, 2004 Fuel Cell Seminar, San Antonio, TX, November, 2004.
[41] United States of America Department of Energy Technical Plan, 2003.
[42] V. Mehta, J.S. Cooper, J. Power Sources 114 (2003) 32–53.
[43] S. Litster, G. McLean, J. Power Sources 130 (2004) 61–67.
[44] E. Antolini, R.R. Passos, E.A. Ticianelli, J. Power Sources 109 (2002) 477–482.
[45] L.R. Jordan, A.K. Shukla, T. Behrsing, N.R. Avery, B.C. Muddle, M. Forsyth, J. Power Sources 86 (2000) 250–254.
[46] J.M. Song, S.Y. Cha, W.M. Lee, J. Power Sources 94 (2001) 78–84.
[47] J. Roth, US Patent Application 2004/0134291 (2004).
[48] R.H. Perry, D.W. Green, J.O.H. Maloney (Eds.), Perry's Chemical Engineers' Handbook, seventh ed., McGraw-Hill, 1997, pp. 6–39.
[49] R.H. Perry, D.W. Green, J.O.H. Maloney (Eds.), Perry's Chemical Engineers' Handbook, seventh ed., McGraw-Hill, 1997, pp. 2–321.
[50] W. Callister Jr., Materials Science and Engineering: An Introduction, John Wiley & Sons, Inc., 1994, p. 646.
[51] K. Hatoh, US Patent 6,210,823 (2001).
[52] J. Benziger, J. Nehlsen, D. Blackwell, T. Brennan, J. Itescu, J. Membr. Sci. 261 (2005) 98–106.
[53] D.P. Wilkinson, J. St-Pierre, in: W. Vielstich, H. Gasteiger, A. Lamm (Eds.), Handbook of Fuel Cells: Fundamentals, Technology and Applications, vol. 3, Wiley, 2003, pp. 611–626.
[54] M. Schulze, T. Knori, A. Schneider, E. Gulzow, J. Power Sources 127 (2004) 222–229.
[55] R. Roshandel, B. Farhanieh, E. Saievar-Iranizad, Renewable Energy 30 (2005) 1557–1572.
[56] K. Cho, S. Kim, J. Lee, S. Um, M. Song, J. Ko, Y. Kim, H. Sim, Y. Sun, 2004 Fuel Cell Seminar Meeting, San Antonio, TX, November, 2004.
[57] US Patent, Application 2004/0058223 (2004).
[58] J.W. Callister, Materials Science and Engineering: An Introduction, John Wiley & Sons, Inc., 1994, p. 496.
[59] J. Scheirs, Compositional and Failure Analysis of Polymers: A Practical Approach, John Wiley & Sons, Inc., 2000, p. 351.